2296.
11. Luck, W. A. P.; Zheng, H. Y. *J. Chem. Soc., Faraday Trans.* **1984**, *80*, 1253.
12. Wohar, M. M.; Seehra, J. K.; Jagodzinski, P. W. *Spectrochimica Acta* **1988**, Vol. 44A, 999.
13. Yaft, R. W. Jr, *Steric effects in organic chemistry*; Newmann, M. S. Ed. (J. Wiley and Son, New York, 1956).

A Statistical Thermodynamic Study on the Conformational Transition of Oligopeptide Multimer

Younggu Kim and Hyungsuk Pak

Department of Chemistry, Seoul National University, Seoul 151-742, Korea
Received July 8, 1995

The conformational transition of oligopeptide multimer, -(HPPHPPP)n-, is studied (H : hydrophobic amino acid, P : hydrophilic amino acid). The helix/coil transitions are detected in the multimer. The transition depends on the number of amino acid in the sequence, the concentration of the oligopeptide, and temperature which affects helix stability constant (ξ) and hydrophobic interaction parameter (w_j). In the thermodynamic equilibrium system $jA \rightarrow A_j$ (where A stands for oligopeptide monomer), Skolnick *et al.*, explained helix/coil transition of dimer by the matrix method using Zimm-Bragg parameters ξ and σ (helix initiation constant). But the matrix method do not fully explain dangling H-bond effects which are important in oligopeptide systems. In this study we propose a general theory of conformational transitions of oligopeptides in which dimer, trimer, or higher multimer coexists. The partition of trimer is derived by using zipper model which account for dangling H-bond effects. The transitions of multimers which have cross-linked S-S bonds or long chains do not occur, because they keep always helical structures. The transitions due to the concentration of the oligopeptides are steeper than those due to the chain length or temperature.

Introduction

The structure and folding of proteins have been actively studied after Pauling and Corey *et al.*[1] discovered α-helical structure of protein in 1951. To understand the folding mechanism of protein and its biological activity, it is necessary to have a knowledge of the spatial coformations. X-ray diffraction has been successful in elucidating the three dimensional structure.[2] However, these crystallographic analyses are quite laborious, expensive, and time consuming. Futhermore many membrane and ribosomal proteins as well as histones, have not yet yielded suitable crystals, so other approaches such as theoretical methods must be explored to give structural information on the basis of experimental data and statistical mechanics.

The theoretical studies on the secondary structure of protein have been done by Chou and Fasmann *et al.*[3] From the tertiary structures of protein solved by X-ray crystallography, they obtained the probabilities of amino acid sequences for α-helical structures, β-sheet, β-turn, and random coils. A study on α-helical structure is more important than any other secondary structures, as α-helical structure amounts up to 80% of many proteins. The regularity of α-helical structure enables a theoretical model to be constructed. As the mean length of α-helix is shorter than 30 residues[4~8] of amino acids, the thermodynamic properties of α-helix in that range are important. Dangling H-bond which exists in the end of α-helix is not important in a long chain, but it must be considered in a short chain in thermodynamic study.

Zimm-Bragg parameters (helix initiation constant and helix stability constant) are insufficient to explain the thermodynamic phenomena of proteins. α-helical structure is determined not only by α-helical H-bonds but also by the species of amino acids and the tertiary interactions surrounding α-carbons of amino acids.[9] The probabilities of amino acids to form α-helices depend on whether they are located inside or surface of protein. The fractional helicity of oligopeptide multimer increases to unity as the concentration of oligopeptide increases.

Skolnick *et al.* derived the partition function of dimer using the matrix method which Zimm *et al.*,[10] and Lifson *et al.*[11] have used and the thermodynamic properties[12~17] of polypeptide. However, this method can not explain dangling H-bond. In this study the thermodynamic functions of polypeptides system, where chain multimers coexist, are derived using zipper model. By this method helix/coil transitions of oligopeptide where dangling H-bonds are important can be well explained.

Theory

The theoretical Study of the conformational Transition of uncross-linked Multimers. Polypeptides-(HPPHPPP)n- are presented as dimer, trimer, tetramer, or higher multimer[18~21] (H : hydrophobic amino acid, P : polar amino acid). In the case of dimer, hydrophobic amino acids are located in a and d position of helical wheel and hydrophobic interactions[22~26] between a-d', a'-d stabilize dimer (Fi-

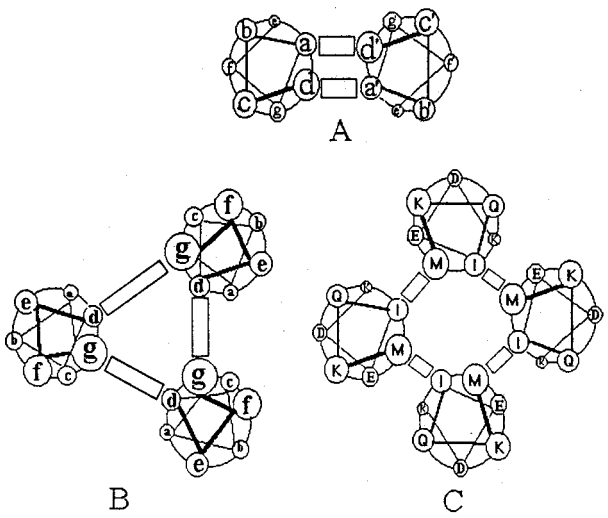

Figure 1. Axial helical projections of dimer(A), cyclic trimer(B), cyclic tetramer(C) in amino ends. In this representation the helicies have been slightly underwound compensate for the left handed supercoiling of structure. Open rectangles stand for hydrophobic interactions between two chains.

gure 1A). For trimer or tetramer, hydrophobic interactions among hydrophobic amino acids stabilize multimer, too (Figure 1B, C).

Multimers have hydrophobic interaction. Let hydrophobic interaction parameter (w_2') in dimer be $\exp(-\Delta G'/RT)$, where $\Delta G_2'$ is the free energy change for the formation of dimer from two monomers. Two turns of σ-helix require seven amino acids. Two hydrophobic interactions of a-d', a'-d between two chains give (w_2').[2] By the mean field theory the free energy change, $2\Delta G_2'$, are uniformly distributed to seven α-carbons of amino acids, then hydrophobic interaction parameter becomes w_2, where $(w_2')^2=w_2^7$ and $2\Delta G_2'=7\Delta G_2$. On the same way hydrophobic interaction parameters in trimer and tetramer are defined as w_3 and w_4, respectively (Figure 1).

The partition function derived through multiple zipper model[27] explains well the properties of polypeptides. However zipper model is enough to illustrate the physical properties of uncross-linked oligopeptide multimers. Uncross-linked multimers are formed by hydrophobic interactions and equilibriums between multimer (A_j) and j monomers (A) are present as follows (Figure 1).

$$\begin{aligned} 2A &\rightarrow A_2 \\ 3A &\rightarrow A_3 \\ &\vdots \\ jA &\rightarrow A_j \\ &\vdots \\ rA &\rightarrow A_r \end{aligned} \tag{1}$$

If C_o is the initial concentration of oligopeptides only consisting of monomer[A] and [A_j] is the concentration of j-mer, then C_o is expressed as follows.

$$C_o=[A]+2[A_2]+3[A_3]+,\cdots+j[A_j]+,\cdots,+r[A_r] \tag{2}$$

Let the mole fraction of oligopeptide consisting of j monomers be g_j and then $[A_j]=C_0\cdot g_j/j$. The chemical equilibrium constant (K_j) is given by

$$K_j=[A_j]/[A]^j \tag{3}$$

$$K_j=\frac{g_j}{g_1^j}\cdot\frac{1}{jC_\sigma^{j-1}} \tag{4}$$

The fractional helicity consisting of uncross-linked multimers is defined as

$$h=\sum_{j=1}^{r} g_j f_j \tag{5}$$

where f_j is the fractional helicity of cross-linked j-mer. The fractional helicity of uncross-linked j-mer is

$$f_j=\frac{\partial \ln Z_j'(N)}{\partial \ln \xi}\cdot\frac{1}{j(N-2)} \tag{6}$$

where $Z'_j(N)$ is the partition function. The chemical equilibrium constant can be given by[28]

$$\begin{aligned} K_j&=V^{j-1}\frac{Z_j(N)}{Z_1(N)^j}=w^{j-1}\frac{(Z_j'(N)-1)}{Z_1(N)^j} \\ &\approx 2w^{j-1}\frac{Z_j'(N)}{Z_1(N)^j} \end{aligned} \tag{7}$$

The partition function ($Z_j(N)$) of oligopeptide consisting of uncross-linked j-mer and g_j can be yielded from eq. 4 and eq. 7. g_j is derived from the relation between the chemical equilibrium constant through partition function and that through the concentrations of the oligopeptide multimers (where $Z_j(N)=(u/V)^j$ $(Z_j'(N)-1)$, $Z_j'(N)\gg 1$). V is the volume of the system, $u=\beta\gamma\pi h(d_{max}^2-d_{min}^2)$[14,29] u being the product of the three factors; (a) the volume of configurational space accessible to the center of mass of one α-helical turn in the dimer when α-helix turn in the other chain is held positional fixed; (b) an orientational factor β that accounts for the relative allowed angular orientation of the α-helical turns that permit the inter helical interaction to occur; (c) the ratio γ of the volume of configurational space spanned by the internal degrees of freedom of the α-helical turn in the dimer to that in the monomers. In order to implement u, we use 5.4 Å for h the length of the α-helical turn, and 7.0 Å for the distance of closest approach,[30] d_{min}, and 14 Å, d_{max},[31] $u=359$ Å^3 for N=29

From eq. 4 we can find

$$g_j=j\cdot C_\sigma^{j-1}\cdot g_1^j\cdot K_j,\quad \sum_{j=1}^{r} g_j=1 \tag{8}$$

Evaluating the partition function of $Z_j(N)$ requires $Z_j'(N)$ of cross-linked multimer. The proportion of the mole fraction of dimer to that of trimer can be estimated through the relation between the equilibrium constants among monomer, dimer, and trimer.

Derivation of Partition Functions of Cross-Linked Trimer. The partition function(Z_2(N)) of cross-linked dimer including end effects has been derived.[32] Several research groups regarded the statistical weight of dangling H-bond as unit. The partition function of all helical oligopeptides is $\sigma\zeta^{N-2}$(N is the number of amino acid residues, N-2 is the number of α-helical H-bonds). The difference between N and N-2 is negligible in a long chain, while it is not negligible in a short chain. That the order of σ is 10^{-4}, makes monozipper model explain well the properties of oligopepti-

Table 1. Partition function of cross-linked trimer when $k=3$, $l=3$: $m=l\text{-}N$: k, l and m stand for the numbers of helical structure for chain 1, chain 2 and chain 3, respectively; helical structures for chain 1 and chain 2 are placed at the amino end

k / l / m / k	structures	statistical	k / l / m / k	structures	statistical
3	hhhcc···cccc		3	chhhc···cccc	
3	hhhcc···cccc	$\sigma^3\xi^3w_3^9$	3	chhhc···cccc	$\sigma^3\xi^4w_3^9$
3	hhhcc···cccc		4	hhhhc···cccc	
3	hhhcc···cccc		3	chhhc···cccc	
3	hhhcc···cccc		3	chhhc···cccc	
3	hhhcc···cccc	$\sigma^3\xi^4w_3^9$	3	chhhc···cccc	$\sigma^3\xi^5w_3^9$
4	hhhhc···cccc		5	hhhhh···cccc	
3	hhhcc···cccc		3	chhhc···cccc	
	···	···		···	···
3	hhhcc···cccc		3	chhhc···cccc	
3	hhhcc···cccc	$\sigma^3\xi^Nw_3^9$	3	chhhc···cccc	$\sigma^3\xi^Nw_3^9$
N	hhhhh···hhhh		N	hhhhh···hhhh	
3	hhhcc···cccc		3	chhhc···cccc	

sum 1 : $\sigma^3w_3^9(\xi^3+\xi^4+\cdots+\xi^N)$ sum 2 : $\sigma^3w_3^9(\xi^4+\xi^4+\cdots+\xi^N)$

$\sum_{m=3}^{N} Z(3,3,m)$: $\sigma_3w_3^9(\xi^3+2\xi^4+3\xi^5+\cdots+(N-2)\xi^N$

des.

On the basis of this assumption, we evaluated the partition of trimer($Z_3(N)$) as follows. Experiments show that leucine zipper peptides such as GCN4-VL, GCN4-LV fall into oligopeptide trimer.[33] The following models are suggested to gain the partition function of oligopeptide trimer. Chain 1 and chain 2 initiate the helical conformation at the same position (Table 1).

Three sequential helical conformations are necessary for one α-helical H-bond model. Summing statistical weight of all possible conformations gives partition function of cross-linked trimer.

k : the number of helical structure chain 1
-h-h-h-c-c-c···c-c-c-c-
hydrophobic interaction
□□□
l : the number of helical structure chain 2
-h-h-h-c-c-c···c-c-c-c-
hydrophobic interaction
□□□
m : the number of helical structure chain 3
-h-h-h-c-c-c···c-c-c-c-
hydrophobic interaction
□□□
k : the number of helical structure chain 1
-h-h-h-c-c-c···c-c-c-c-

model 1

In model 1, the statistical weight is $\sigma^3\zeta^9\omega^9$ when dangling H-bonds are not included. However, it is $\sigma^3\zeta^3\omega^9$ when dangling H-bonds are. The assumptions of model 1 are as follows. Helices are initiated at amino terminals of chain 1, chain 2, and chain 3, respectively. The number of helical structures of chain 1 is $k=3$ and that of chain 2 is $l=3$, that of chain 3 is $m=3, 4,\cdots, N$.

The sum 1 in Table 1 constructed by model 1 is

$$\sigma^3w_3{}'9(\xi^3+\xi^4+\xi^5+\cdots+\xi^N) \tag{9-1}$$

The sum 2 in Table 1 is obtained as follows. The positions of helix initiation of chain 1 and chain 2 are shifted by one residue. The number of helical structures is $m(=4, 5,\cdots, N)$ and its partition function is given by eq. 9-2. We have obtained the partition function with carrying the position of helix initiation, one by one, from the amino end to the carboxyl end.

$$\sigma^3w_3^9(\xi^4+\xi^5+\cdots+\xi^N) \tag{9-2}$$
$$\vdots$$
$$\sigma^3w_3^9\xi^N \tag{9-N}$$

Summing the above results is

$$\sum_{m=3}^{N} Z(3,3,m)=\sigma^3w_3{}^0(\xi^3+2\xi^4+3\xi^5+\cdots+(N-2)\xi^{(N-3)}) \tag{10}$$

Likewise we obtain the subsidiary equation ($k=3$, $l=4$)

$$\sum_{m=3}^{N} Z(3,4,m)=\sigma^3w_3^9(\xi^5+2\xi^6+3\xi^7+\cdots+(N-3)\xi^{(N+1)}) \tag{11}$$

In general, $\sum_{l=3}^{N}\sum_{m=3}^{N} Z(k,l,m)$ is given by

$$\sigma^3w_3{}^{3k}(\xi^{(3k-6)}+2\xi^{(3k-5)}+3\xi^{(3k-4)}+4\xi^{(3k-3)}+\cdots +(N-l+1)\xi^{(N+2k-6)}) \tag{12}$$
$$\vdots$$
$$\sigma^3w_3{}^{(2k+l)}(\xi^{(3k-6)}+2\xi^{(3k-5)}+3\xi^{(3k-4)}+4\xi^{(3k-3)}+\cdots +(N-l+1)\xi^{(N+2k-5)}) \tag{13}$$
$$\vdots$$
$$\sigma^3w_3{}^{(2k+N)}\xi^{(3k-6)} \tag{14}$$

where $l=k\text{-}N$, $m=l\text{-}N$.

The partition functions of cross-linked trimer after summing of eq. 12-eq. 14, is approximately given by

$$Z_3(N)\approx 1+\sum_{k=3}^{N}\sum_{l=k}^{N}\sum_{m=l}^{N}(m-l+1)\sigma^3\xi^{(3k+m-l-6)}w_3{}^{(2k+l)} \tag{15}$$

The partition function of eq. 15 is illustrated by model 2 where the number of hydrophobic interactions is maximized. The number of hydrophobic interaction in model 3 is smaller by two than in model 2 with moving the position of helix initiation as many as one from amino end to carboxyl end.

chain 1 ccccchhhhccccccc
chain 2 ccccchhhhccccccc
chain 3 ccccchhhhccccccc
chain 1 ccccchhhhccccccc

model 2

chain 1 ccccchhhhccccccc	chain 1 ccccchhhhccccccc
chain 2 ccccchhhhccccccc	chain 2 ccccchhhhccccccc
chain 3 ccccchhhhccccccc	chain 3 ccccccchhhhccccc
chain 1 ccccchhhhccccccc	chain 1 ccccchhhhccccccc

model 3

chain 1 ccccchhhhccccccc	chain 1 ccccchhhhccccccc
chain 2 ccccchhhhccccccc	chain 2 ccccchhhhccccccc
chain 3 ccchhhhccccccc	chain 3 cccccchhhhcccc
chain 1 ccccchhhhccccccc	chain 1 ccccchhhhccccccc

model 4

Model 2 is modified by adding model 3 and model 4, and the partition function of trimer is obtained as

$$Z_3(N)=1+\sum_{k=3}^{N}\sum_{l=k}^{N}\sum_{m=l}^{N}(m-l+1)\sigma^3\xi^{(3k+m-l-6)}w_3^{(2k+l)}+2\sum_{k=3}^{N}\sum_{l=k}^{N}\sum_{m=l}^{N}(m-l+1)\sigma^3\xi^{(3k-m-l-6)}w_3^{(2k+l-2)}+2\sum_{k=3}^{N}\sum_{l=k}^{N}\sum_{m=l}^{N}(m-l+1)\sigma^3\xi^{(3k-m-l-6)}w_3^{(2k+l-4)} \quad (16)$$

The first term of eq. 16, unit, is the stastical weight when chain 1, chain 2, and chain 3 are all coil conformations. The second term (model 2) is the sum of states when the number of hydrophobic amino acids interacting each other is largest in chain 1, chain 2 and chain 3. The third term (model 3) and last term (model4) are the sum of states when that is fewer by two and four than in model 2, respectively.

Differentiating eq. 16 we have

$$h_3=\frac{\partial \ln Z_3(N)}{\partial \ln \xi}\cdot\frac{1}{(3N-6)} \quad (17)$$

The thermodynamic Properties of the Chemical Equilibrium between Uncross-linked Dimer and Trimer. If oligopeptides exist only monomer, dimer and trimer, the following chemical equilibrium are

$$2A \rightleftarrows A_2,\ K_2=[A_2]/[A]^2 \quad (18)$$

$$3A \rightleftarrows A_3,\ K_3=[A_3]/[A]^3 \quad (19)$$

The chemical equilibrium constants are also derived by statistical mechanics.

$$K_2=\frac{uZ_2(N)}{Z_1(N)^2} \quad (20)$$

$$K_3=\frac{u^2Z_3(N)}{Z_1(N)^3} \quad (21)$$

Let g_k be the mole fraction of species(A_k). Then

$$\sum_{k=1}^{3}g_k=1 \quad (22)$$

$$[A]=C_o g_1,\ [A_2]=\frac{C_o g_2}{2},\ [A_3]=\frac{C_o g_3}{3} \quad (23)$$

By inserting $g_2=2C_o g_1^2K_2$ and $g_3=3C_o^2g_1^3K_3$ into eq. 22 and rewriting of eq. 22, we find

$$g_1+2C_o g_1^2K_2+3C_o^2g_1^3K_3=1 \quad (24)$$

The fractional helicity(h) is expressed by

$$h=g_1h_1+g_2h_2+g_3h_3=g_1h_1+2C_o g_1^2K_2h_2+3C_o^2g_1^3K_3h_3 \quad (25)$$

In eq. 25, the first, second and the third terms stand for the fractional helicity of monomer, dimer, and trimer, respectively. The fractional helicities have been assumed to be independent of concentration. Differentiating eq. 25 with respect to the concentration is given by

$$\frac{dh}{d\ln C_o}=\frac{dg_1}{d\ln C_o}h_1+\frac{dg_2}{d\ln C_o}h_2+\frac{dg_3}{d\ln C_o}h_3 \quad (26)$$

where $\frac{dg_1}{d\ln C_o}$, $\frac{dg_2}{d\ln C_o}$ and $\frac{dg_3}{d\ln C_o}$ are given as follows

$$\frac{dg_1}{d\ln C_o}=\frac{-2(K_2+3C_o g_1K_3)C_o g_1^2}{1+4C_o g_1K_2+9C_o^2g_1^2K_3} \quad (27)$$

$$\frac{dg_2}{d\ln C_o}=2g_1C_oK_2\left(g_1+2\frac{dg_1}{d\ln C_o}\right) \quad (28)$$

$$\frac{dg_3}{d\ln C_o}=3g_1^2C_o^2K_3\left(2g_1+3g_1^2\frac{dg_1}{d\ln C_o}\right) \quad (29)$$

Differentiating eq. 25 with respect to temperature, we obtain

$$\frac{dh}{dT}=h_1\frac{dg_1}{dT}+g_1\frac{dh_1}{dT}+4C_o g_1h_2K_2\frac{dg_1}{dT}+2C_o g_1^2h_2\frac{dK_2}{dT}+2C_o g_1^2h_2K_2\frac{dh_2}{dT}+9C_o^2g_1h_3K_3\frac{dg_1}{dT}+3C_o^2g_1^3h_3\frac{dK_3}{dT}+3C_o^2g_1^3K_3\frac{dh_3}{dT} \quad (30)$$

Differentiating the chemical equilibrium constants with respect to temperature, we obtain the van't Hoff equation as follows;

$$\frac{d\ln K_2}{dT}=\frac{\Delta H_2}{RT^2}=\frac{d\ln Z_2(N)}{dT}-2\frac{d\ln Z_1(Z)}{dT} \quad (31)$$

$$\frac{d\ln K_3}{dT}=\frac{\Delta H_3}{RT^2}=\frac{d\ln Z_3(N)}{dT}-3\frac{d\ln Z_1(Z)}{dT} \quad (32)$$

where ΔH_2 and ΔH_3 are the enthalpy changes when 2 mole and 3 mole of A are transformed to A_2 and A_3, respectively. The dependence of the fractional helicities on temperature is derived through eq. 30, eq. 31 and eq. 32.

Result and Discussion

Determination of Zimm-Bragg parameters. Let σ_{Bi} and ζ_{Bi} be the helix initiation constant and the helix stability constant of homo-oligopeptide consisting of amino acid B_i, respectively. By the mean field theory the helix initiation constant and the helix stability constant of oligopeptide (B_1-B_2-$\cdots$-B_N) are given by

$$\sigma=\prod_{i=1}^{N}(\sigma_{Bi})^{1/N},\ \zeta=\prod_{i=1}^{N}(\zeta_{Bi})^{1/N},$$

respectively. Zimm-Bragg parameters[34~53] of homo-oligomers are shown in Table 2. From the relation between ξ and $\Delta S=-17.5$ J/molK,[54~57] ($\xi=\exp(-\Delta H/RT+\Delta S/R)$)$\Delta H$ can be calculated where ΔH and ΔS are the change of enthalpy and that of entropy from random coil to helix structure per one mole of oligopeptide, respectively. Zimm-Bragg parameters of α tropomycin and GCN4-proteins obtained through Table 3 are shown in Table 2.

Determination of Hydrophobic Interaction Parameters and their Properties. Hydrophobic interaction parameters have been determined as follows; Having tropo-

Table 2. Zimm-Bragg parameters and enthalpy change of some oligopeptides at 20 ℃

	α tropomycin	GCN4-p1	GCN4-VL	GCN4-LV
$\sigma(\times 10^4)$	5.00	6.57	6.22	6.22
ζ	0.970	1.01	0.967	0.967
ΔH (kJ/mol)	−5.14	−5.15	−5.13	−5.13

Table 3. Predicted thermodynamic parameters for the secondary structures of homopolypeptide residue at 20 ℃

polypeptide	ζ	σ ($\times 10^4$)	Reference
poly-ala	1.07	8.0	34
poly-val	0.95	1.0	35
poly-leu	1.14	33.	36
poly-ile	1.14	55.	37
poly-pro	0.27	0.1	38
poly-met	1.20	54.	39
poly-phe	1.09	18.	40
poly-trp	1.11	77.	41
poly-gly	0.59	0.1	42
poly-ser	0.76	0.1	43
poly-thr	0.82	0.1	44
poly-cys	0.99	1.0	45
poly-tyr	1.02	66.	46
poly-asn	0.78	0.1	47
poly-gln	0.98	33.	48
poly-asp	0.78	210.	49
poly-glu	1.35	100.	50
poly-lys	0.94	1.0	51
poly-arg	1.03	0.1	52
poly-his	0.85	210.	53

mycin cut to N=43, the fractional helicity of tropomycin oligopeptide have been evaluated through experiments.[24] and w_2, through the numerical methods.[23~26]

$$RT\ln w_2 = BT\ln T + A_0 + A_1 T + A_2 T^2 \quad (33)$$

Skolnick *et al.* have evaluated the coefficients, B=52.627, A_0=15793.5, A_1=−351.163, A_2=0.00 by using the matrix method at pH=7.4. In this study the coefficients of hydrophobic interactions are elicited from the experimental data of Skolnick *et al.*'s by using the zipper model that includes the end effects. The coefficients of ours are shown in Table 4; B=52.58, A_0=16191.0, A_1=−351.912, A_2=0.00 (R=0.082 cal/mol K). The values of the coefficients are close to Skolnick *et al.*'s except A_0. There are little differences in the coefficients of hydrophobic interaction parameters between ours and theirs in α tropomycin and GCN4-p1, however those of GCN4-VL with high melting temperature are very large. Inserting the values shown in Table 1 into eq. 33, the variations of w_2 and w_3 with temperature have been obtained. w_2 of tropomycin and GCN4-p1 protein in the range of 0 ℃-100 ℃ are 3.35-2.69, 3.79-3.57 and the minimum of w_2 of those are 34 ℃, and 36 ℃, respectively.

In this study the plot of RTln$w$ *vs.* temperature (pH 7.4)

Table 4. Coefficients of hydrophobic interaction parameter (N=31)

	α tropomycin	GCN4-p1	GCN4-VL	GCN4-LV
dimer B	52.584	51.1271	48.992	.
dimer A_0	16191.0	15975.0	18678.0	.
dimer A_1	−351.912	−342.663	−337.185	.
trimer B	.	.	28.595	28.72
trimer A_0	.	.	107.51	10487.
trimer A_1	.	.	−196.515	−196.515
T_m (℃)	31.	53.	95.	81.

The values of A_2 is zero for all cases and T_m stands for the midpoint of thermal transition of oligopeptides.

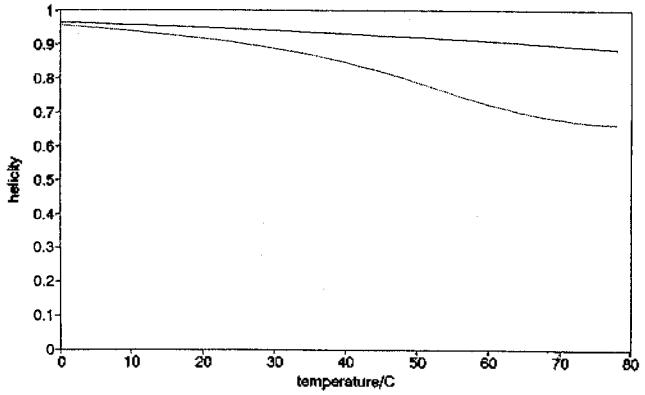

Figure 2. Helicity *vs.* temperature for cross-linked oligopeptides. Solid curve: GCN4-p1, Dotted curve: α tropomycin.

of α tropomycin is very different from that obtained by Skolnick *et al.* These results presumably come from differences between our model considered in dangling H-bond and theirs not considered in dangling H-bond. In general the hydrophobic interaction is in proportion to temperature. However our results show that it is not. These phenomena presumably come from the electrostatic interactions (e' and g), the concentration of proton, and solvent effects (Figure 1). The melting occurs gradually where w_2 and w_3 have minimum in dimer and trimer, respectively. The values of hydrophobic interaction parameters (w_2) for GCN-VL(T_m=95 ℃) are 2.98 at 40 ℃ and 2.28 at 100 ℃ and those for GCN-LV (T_m=81 ℃), 2.75 at 40 ℃, 2.18 at 93 ℃ and 2.19 at 100 ℃.

Fractional helicity of multimer as temperature. The fractional helicity of the cross-linked multimer[13] is independent of the concentration of oligopeptides. The fractional helicity of α tropomycin is 0.95-0.65 in the ranges of 0 ℃-78 ℃, that of GCN4-p1, 0.96-0.87, that of GCN4-VL, larger than 0.89, and that of GCN4-LV, larger than 0.81 (Figure 2). Proteins such as uncross-linked GCN4-p1 and α tropomycin (N≤43) are melted less than 95 ℃. The denaturations of the cross-linked proteins with respect to temperature is difficult to occur.

Dissociation of multimer as temperature. The fractional helicity of dimer or trimer are greatly affected by the helix stability constant, the helix initiation constant, and

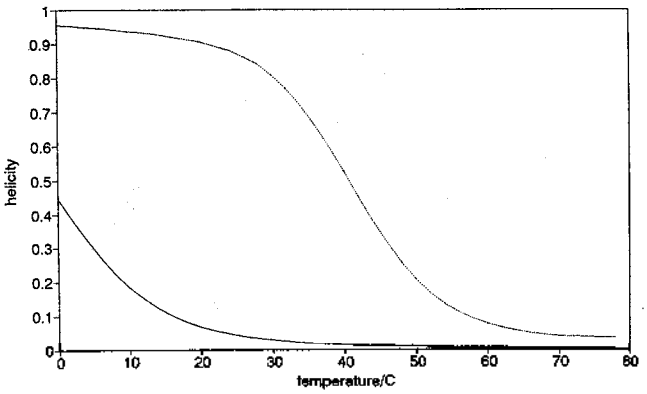

Figure 3. Helicity *vs.* temperature for noncross-linked α tropomycin. The concentration of α tropomycin is 150 μM. (N=31) Dotted curve: noncrossed-linked dimer. Soild curve: monomer.

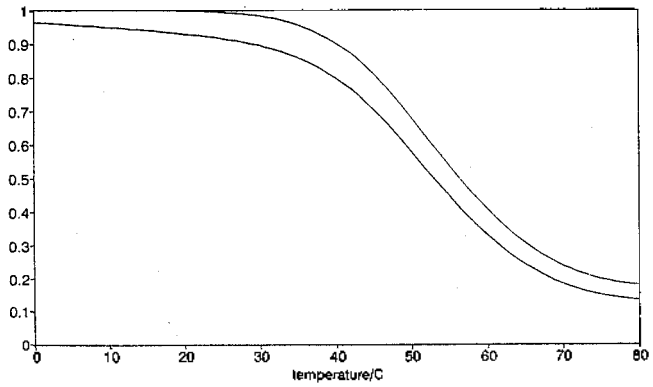

Figure 4. Helicity and mole fraction of dimer *vs.* temperature for non-cross-linked GCN4-p1, at N=31. The concentration of GCN4-p1 is 150 μM. Dotted curve: mole fraction of dimer (g_2). Solid curve: helicity of noncrossed-linked GCN4-p1.

the hydrophobic interaction parameter. Among them the helix stability constant and hydrophobic interaction parameters are deeply affected by temperature.

The transition temperature of α tropomycin at 8.19×10^{-7} M (N=43) is 53 ℃.[24] The longer chain is, the smoother slope of fractional helicity is. The transition occurs rapidly at 22 ℃ where N=29, $C_o=8.19\times10^{-7}$ M. α tropomycin (T_m=41 ℃), GCN4-p1 (T_m=53 ℃) are always dimer at 150 μM, (N=31) (Figure 3). The higher melting temperature of GCN4-p1 than that of α tropomycin indicates that the α-helicies of GCN4-p1 are more stable than that of tropomycin. The slope of the fractional helicity of GCN4-p1 with respect to temperature is slower than that of α tropomycin. High T_ms value of GCN4-VL and GCN4-LV show that the helix structures of GCN4-VL and GCN4-LV are very stable. The facts that GCN4-VL melts at high temperature are explained as follows; Decreasing the rate of helix stability constant is larger than the increasing rate of hydrophobic interaction parameter for temperature (Figure 4, 5).

Fractional helicity as Concentration of Oligopeptides. If the concentration of oligopeptide is low enough ($C_o<10^{-9}$ M), all chains are monomers. But if that of oligopeptide is denser than 8.19×10^{-7} M, the fractional helicity

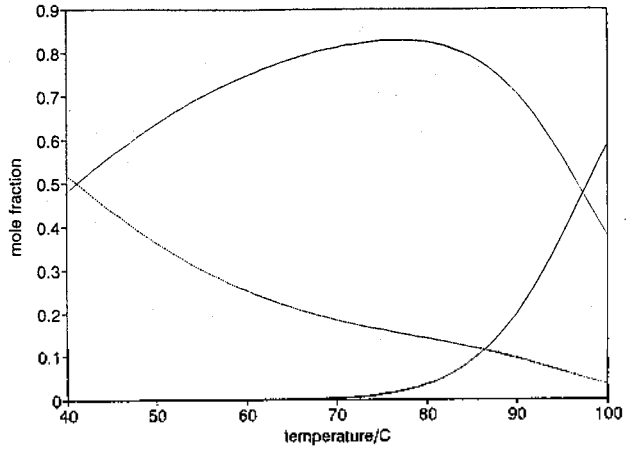

Figure 5. Mole fractions *vs.* temperature for noncross-linked GCN4-VL. Dotted curve: monomer, Solid curve: dimer. Dashed curve: trimer.

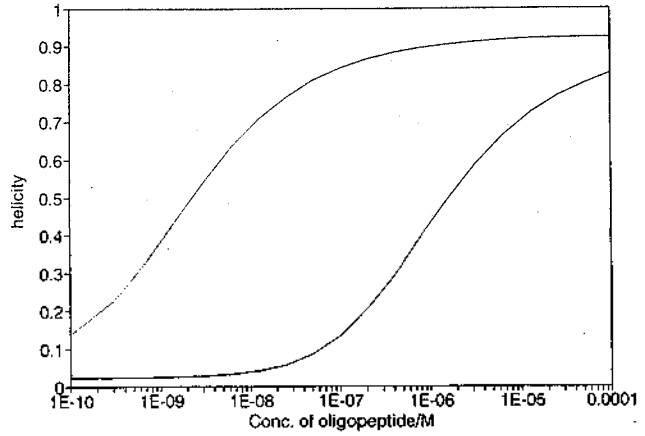

Figure 6. Helicity vs. concentration of noncross-linked GCN4-p1(N=31). Dotted: 22 ℃. Solid curve at 37 ℃.

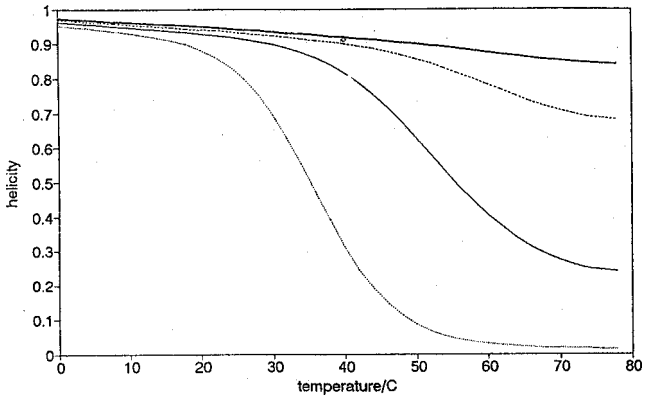

Figure 7. Helicity *vs.* temprature and the length of α tropomycin. The concentration of α tropomycin is 150 μM. Dotted: N=29. Solid curve: N=36. Dashed curve: N=43 Heavy solid curve: N=50.

is larger than 0.96. The transition for the concentration of oligopeptide is sharper than that of temperature. If the con-

centration of α tropomycin or GCN4-protein is beyond 10^{-6} M, they maintain helical structure at room temperature. α tropomycin (N=31) has a rapid transition at 3.10×10^{-9} M (37 ℃), GCN4-p1 protein (N=31) at 3.4×10^{-9} M (22 ℃), and 1.64×10^{-6} M (37 ℃). GCN4-VL has a rapid transition at 5.2×10^{-9} M and 70 ℃ (Figure 6).

Transition temperature as chain length. The transition of α tropomycin and GCN4-p1 in a long chain does not occur even at high temperature. α tropomycin (N=39) has helix/coil transition at 70 ℃, but a long chain (N>39) has not. GCN4-p1(N=35) has helix/coil transition at 70 ℃, but the longer chain has not (Figure 7).

Conclusion

Polypeptide, (HPPHPPP)n-, theoretically has many species of multimers. The general formula for the mole fractions of multimers are obtained from the relation between chemical equilibrium constants through the concentration of polypeptide and that through partition function. The partition functions which include end effects for dimer or trimer can be derived with zipper model, but can not be with the matrix method. From the partition function of α tropomycin, hydrophobic interaction parameters are obtained. These results are little different from those of Skolnick *et al.*'s except A_0. And hydrophobic interaction parameters of other oligopeptides (*eg.* GCN4-p1, GCN4-VL, GCN4-LV) have been obtained. Hydrophobic interaction energy is the dominant force of protein folding or oligopeptide multimerization.[58~62] Statistical thermodynamic equations for those energies have not been known, but those energies of small molecules (*eg.* H_2O)[63] are in proportion to temperature. In this study α tropomycin and GCN4-proteins agrees well with the published data, but the other proteins do not.

Not only hydrophobic interactions but electrostatic interactions between hydrophilic amino acids exist in oligopeptides multimers. At the denaturating temperature and concentration of protein, denaturation of tertiary structure of protein and secondary structures/coil transition occur simultaneously (Figure 4 and Figure 5). It indicates that dissociations of oligopeptide multimers determine the helix/coil transition. That the helicity of the cross-linked dimer is large at high temperature, shows that the cross-linked protein must be very stable. Secondary structure/coil transition[64] of a concentrated solution or a long chain oligopetide cannot be detected at even high temperature. In general transition through temperature are relatively smoother than through the concentration of oligopeptide.

In this study thermodynamic properties of dimer and trimer are investigated. Comparison these with the experimental data such as solution light scattering, CD spectroscopy, and ultracentrifuge will give useful informations of multimers.[65~67]

Acknowledgment. The present Studies were Supported (in part) by the Basic Science Institute program, Ministry of Education, 1995. Project No. BSRI-95-3414.

References

1. Pauling, L.; Corey, R. B.; Branson, H. R. *Proc. Natl. Acad. Sci.* USA **1951**, *30*, 205.
2. *Protein Data Bank* #67 Quaterly Newsletter Jan 1994.
3. Chou, P. Y.; Fasman, G. D. *Ann. Rev. Bioch.* **1978**, *47*, 251.
4. Morisnaga, T.; Funatsu, G.; Funatsu, M.; Wittmann, H. G. *FEBS Lett.* **1976**, *64*, 307.
5. Chen, R.; Ehrke, G. *FEBS Lett.* **1976**, *69*, 240.
6. Clotz, I. M.; Klippenstein, G. L.; Hendrickson, M. A. *Science* **1976**, *192*, 335.
7. Robson, B. *Biochem. J.* **1974**, *141*, 853.
8. Venkatachalan, C. M. *Biopolymers* **1968**, *6*, 1425.
9. Beyreuther, K.; Adler, K.; Geisler, N.; Klemm, A. *Proc. Natl. Acad. Sci. USA* **1993**, *70*, 3526.
10. Zimm, B. H.; Bragg, J. K. *J. Chem. Phys.* **1959**, *31*, 526.
11. Lifson, S.; Loig, A. *J. Chem. Phys.* **1961**, *34*, 1963.
12. Holtzer, M. E.; Holtzer, A.; Skolnick, J. *Macromolecules* **1983**, *16*. 173.
13. Skolnick, J. *Macromolecules* **1984**, *17*, 2153.
14. Skolnick, J. *Macromolecules* **1984**, *17*, 2158.
15. Skolnick, J. *Macromolecules* **1985**, *18*, 1535.
16. Skolnick, J.; Holtzer, A. *Macromolecules* **1985**, *18*, 1549.
17. Skolnick, J. *Macromolecules* **1986**, *19*, 1153.
18. Habury, P. B.; Zhang, T.; Kim, P. S.; Alber, T. *Science* **1993**, *262*, 1401.
19. Fairman, R.; Spencer, J. A.; Degrado, W. F. *J. Amer. Chem. Sci.* **1992**, *114*, 5458.
20. O'Neil, K. T.; Degrado, W. F. *Science* **1990**, *250*, 646.
21. Skolnick, J.; Holtzer, A. *Macromolecules* **1982**, *15*, 303.
22. Cohen, C.; Szent-Gyorgyri, A. G. *J. Amer. Chem. Sci.* **1957**, *79*, 248.
23. Holtzer, A.; Clark, R.; Lowey, S. *Biochemistry* **1965**, *4*, 2401.
24. (a) Woods, E. *Aust. J. Biol. Sci.* **1976**, *29*, 405. (b) Crmmins, D.; Isom, L.; Holtzer, A. *Comp. Biochem. Physiolo.* **1981**, *69B*, 35.
25. Wu, C. S.; Ikeda, K.; Yang, J. T. *Biochemistry* **1981**, *20*, 566.
26. Mattice, W. L. *Biopolymers* **1985**, *24*, 2331.
27. Kim, Y.; Pak, H. *J. Kor. Chemi. Sci.* **1994**, *38(10)*, 710.
28. Mayer, J., Mayer, M. *Statistical Mechanics*; Wiely, New York, 1940, p 215.
29. Lehmann, G. W.; Mctague, J. P. *J. Chem. Phys.* **1968**, *49*, 3170.
30. Chou, K.-C.; Nemethy, G.; Scheraga, H. *J. Phys. Chemi.* **1983**, *87*, 2869.
31. Phillips, G. *Biophys. J.* **1984**, *45*, 392a.
32. Kim, Y.; Pak, H. To be published at *J. Kor. Chemi. Sci.* **1995**.
33. Arnott, S.; Wonacott, A. J. *J. Mol. Biol.* **1966**, *21*, 371.
34. Plater, K. E. B.; Annathanarayanan, V. S.; Andreatta, R. H.; Sheraga, H. A. *Macromolecules* **1972**, *5*, 177.
35. Alter, J. E.; Andrenatta, R. H; Taylor, T.; Sheraga, H. A. *Macromolecules* **1973**, *6*, 564.
36. Allgra, G. *J. Polym. Sci. Part C* **1967**, *16*, 2815.
37. Fredickson, R. A.; Chang, M. C.; Powers, S. P.; Sheraga, H. A. *Macromolecules* **1981**, *14*, 625.
38. Altmann, K. H.; Wojcik, J.; Vasqeuz, M.; Sheraga, H. A. *Biopolymers* **1990**, *30*, 107.
39. Hill, D. J. T.; Cardinaux, F.; Sheraga, H. A. *Biopolymers* **1977**, *16*, 2447.
40. van Wart, R. E.; Taylor, G. T.; Sheraga, H. A. *Macromolecules* **1973**, *6*, 266.

41. Nagy, J. A.; Powers, S. P.; Zweifel, B. O.; Sheraga, H. A. *Macromolecules* **1980**, *13*, 1428.
42. Annathanarayanan, V. S.; Andreatta, R. H.; Poland, D.; Sheraga, H. A. *Macromolecules* **1971**, *4*, 417.
43. Hughes, L. J.; Andreatta, R. H.; Sheraga, H. A. *Macromolecules* **1972**, *6*, 266.
44. Mecht, M. H.; Zweifel, B. O.; Sheraga, H. A. *Macromolecules* **1978**, *11*, 545.
45. Wojcik, J.; Altmann, K. H.; Sheraga, H. A. *Biopolymers* **1990**, *30*, 121.
46. Scheule, R. K.; Cardinaux, F.; Taylor, G. T.; Sheraga, H. A. *Macromolecules* **1976**, *9*, 23.
47. Matheson, R. R.; Jr. Nemenoff, R. A.; Cardinaux, F.; Sheraga, H. A. *Biopolymers* **1977**, *16*, 1517.
48. Denton, J. B.; Powers, S. P.; Zweifel, B. O.; Sheraga, H. A. *Biopolymers* **1982**, *21*, 51.
49. Kobayachi, Y.; Cardinaux, F.; Zweifel, B. O.; Sheraga, H. A. *Macromolecules* **1977**, *10*, 1271.
50. Maxfeld, F. R.; Alter, J. E.; Taylor, G. T.; Sheraga, H. A. *Macromolecules* **1975**, *8*, 479.
51. Konishi, Y.; van Nispen, J. W.; Daveport, G. D.; Sheraga, H. A. *Macromolecules* **1977**, *10*, 1264.
52. Ingall, R. T.; Sheraga, H. A.; Lotan, V.; Berger, A.; Katachaski, E. *Biopolymers* **1968**, *6*, 331.
53. Sueki, M.; Lee, S.; Powers, S. P.; Denton, J. B.; Konishi, Y.; Sheraga, H. A. *Macromolecules* **1984**, *17*, 148.
54. Schellman, J. A. *C. R. Trav. Lab. Carsberg Ser. Chim.* **1955**, *29*, 223.
55. Baldwin, R. L. *Proc. Natl. Acad. Sci. USA* **1986**, *83*, 8069.
56. Privalov, P. L. *Adv. Protein Chem.* **1979**, *33*, 167.
57. Murphy, K. P.; Privalov, P. L.; Gill, S. J. *Science* **1990**, *247*, 559.
58. Kausmann, W. *Adv. Protein Chem.* **1959**, *16*, 1.
59. Nemthy, G.; Scheraga, H. A. *J. Chem. Phys.* **1962**, *36*, 3382.
60. Rose, G. D.; Wolfenden, R. *Ann. Rev. Biomol. Struct.* **1993**, *22*, 381.
61. Dill, K. A. *Biochemistry* **1985**, *24*, 1501.
62. Dill, K. A. *Biochemistry* **1990**, *29*, 7133.
63. Pratt, L. R.; Chandler, D. *J. Chem. Phys.* **1977**, *67*, 3683.
64. Lovejoy, B.; Choe, S.; Cascio, D.; Mcrorie, D. K.; Degrado, W. F.; Einsenberg, D. *Science* **1993**, *259*, 1288.
65. Raleigh, D. P.; Degrado, W. F. *J. Amer. Chem. Sci.* **1992**, *114*, 10079.
66. Grove, A.; Mutter, M.; Riviver, J. E.; Montal, M. *J. Amer. Chem. Sci.* **1993**, *115*, 5919.
67. Hu, Y.; Chin, T. M.; Fleming, G. R.; Yang, N. C. *J. Phys. Chem.* **1993**, *97*, 1330.

Kinetics and Mechanism of Substitution Reaction of $PPN^+(\eta^5\text{-MeCp})Mn(CO)_2Cl^-$ with PR_3 (R=Me, Et, OEt, C_6H_5)

Yong Kwang Park*, Yong Gu Lee, and Gyu Shik Kim*

*Department of Chemistry, *Department of Science Education, Kangwon National University, Chuncheon 200-701, Korea*

Received July 25, 1995

The transition metal carbonylate, $PPN^+(\eta^5\text{-MeCp})Mn(CO)_2Cl^-$ undergoes a novel ligand substitution reaction with PR_3 (R=Me, Et, OEt, C_6H_5) in THF at elevated temperatures (40 ℃ up to 60 ℃) under the pseudo-first-order reaction conditions (usually 20-fold excess of PR_3 with respect to metal carbonylate concentrations) where chloride is displaced by PR_3. The reaction follows overall first order dependence on $[(\eta^5\text{-MeCp})Mn(CO)_2Cl^-]$; however, the negative entropy changes of activation ($\Delta S^\ddagger = -19.3$ e.u. for $P(OEt)_3$; $\Delta S^\ddagger = -16.4$ e.u. for PPh_3) suggest the existence of the intermediate, $(\eta^3\text{-MeCp})Mn(CO)_2(THF)Cl^-$, which eventually transforms to the product $(\eta^5\text{-MeCp})Mn(CO)_2(PR_3)$.

Introduction

For the last decades, many chemists observed the nucleophilicity of the transition metal carbonylates toward organic halides and also studied the counterion effect on the reaction.[1] The displacement of X^- from RX (X^-=halides) by metal carbonylates usually follows an overall second order rate law, rate=$k_2[M(CO)_x^-][RX]$ for the reaction (1).

$$M(CO)_x^- + RX \rightarrow RM(CO)_x + X^- \quad (1)$$

The metal carbonylate, however, does not undergo a ligand substitution reaction with PR_3 at elevated temperatures probably due to the strong $d\pi$-$p\pi^*$ back-bonding between the metal and the carbonyl carbon. Several years ago we reported on the reaction of $M^+[M'M''(CO)_9L]^-$ ($M^+=Na^+$, PPN^+; M'=Cr, W; M''=Mn, Re; L=CO, PR_3) with PR_3, where the heterobimetallic complex contains a donor-acceptor metal-metal bond.[2]

In this case, however, ligand substitution reaction could be accomplished by relieving the high electron density on Mn onto the Lewis acid moiety, $M(CO)_5$ (M=Cr, W), as shown in equation (2).

$$(OC)_5CrMn(CO)_5^- + PR_3 \rightarrow Mn(CO)_5^- + Cr(CO)_5PR_3 \text{ (major)} + Cr(CO)_4(PR_3)_2 \text{ (minor)} \quad (2)$$

Tremendous amount of research on the ligand substitution reaction of the neutral metal carbonyl with PR_3 has been performed in the last twenty years including the following reaction as shown in equation (3).[3]

$$Mn(CO)_5Br + PR_3 \rightarrow cis\text{-}Mn(CO)_4(PR_3)Br + CO \quad (3)$$

Here we report a rare ligand substitution reaction in which the metal carbonylate $(\eta^5\text{-MeCp})Mn(CO)_2Cl^-$ shows Cl^-/PR_3 exchange leading to the product, $(\eta^5\text{-MeCp})Mn(CO)_2(PR_3)$. From the ligand substitution kinetics, the reaction mechanism will be discussed in detail.

Experimental

All operations were carried out under a nitrogen atmosphere by using standard Schlenk techniques or an Ar-filled glovebox. Rigorous exclusion of trace moisture and oxygen was standard procedure. Solvents were dried and degassed as described below. Infrared spectra were recorded on a Perkin-Elmer 283 spectrophotometer using 0.10-mm sealed CaF_2 or KBr solution cells. ^1H NMR spectra were obtained from Varian Gemini-200 FT spectrometer in solutions of $CDCl_3$, DMSO-d_6, and CD_3OD. The GC-MASS spectral data were collected from the GC-MASS (Hewlett Packard model GC 5890), Department of Chemistry Yonsei University (Wonju, Kangwondo). Photoreactions were performed by using a 450 watt Hg vapor lamp (Hanovia).

Tetrahydrofuran (THF) was distilled under nitrogen from purple sodium/benzophenone ketyl. Hexane was stirred over concentrated H_2SO_4 overnight, washed with aqueous $NaHCO_3$ and distilled from Na^0/benzophenone ketyl. Methylene chloride was refluxed over calcium hydride and distilled under N_2. Ethanol and methanol were distilled from calcium hydride. Bis(triphenylphosphine)iminium chloride (PPN^+Cl^-) was purchased from Aldrich. All other reagents purchased were reagent grade and used without further purification.

Preparation of $(\eta^5\text{-MeCp})Mn(CO)_2(THF)$. The preparation procedure of $(\eta^5\text{-MeCp})Mn(CO)_2(THF)$ is similar to a method in the literature.[4]

Preparation of $PPN^+(\eta^5\text{-MeCp})Mn(CO)_2Cl^-$. To a N_2-filled 100 mL Schlenk flask PPN^+Cl^- (1.20 mmol) was loaded. The system was evacuated for 1 hr and then back-filled with N_2. A 10 mL portion of degassed dichloromethane was added *via* a syringe and the solution stirred for several minutes. To the PPN^+Cl^- (1.20 mmol) solution was added a THF solution (30 mL) of $(\eta^5\text{-MeCp})Mn(CO)_2(THF)$ (1.0 mmol) freshly prepared from the photolytic reaction. This solution was stirred for 1 hr at room temperature and then the solution was concentrated to 20 mL under vacuum. Hexane (50 mL) was slowly added to precipitate the product and the mother liquid was removed via cannula. The solid was washed with hexane until the washings were colorless. After removal of the hexane, the solid product was redissolved in THF (20 mL) and passed through Celite-containing glass filter. Hexane was slowly added to the solution as the precipitation began. The fine red brown solid was separated and dried in vacuo to give 0.5 mmol of the product (50% yield).

$PPN^+(\eta^5\text{-MeCp})Mn(CO)_2Cl^-$. ν(CO)IR (THF) in cm^{-1}, 1893 (s), 1816 (s). Anal. Calcd for $C_{44}H_{37}NO_2P_2Cl$: C, 69.16; H, 4.88; N, 1.83. Found: C, 69.42; H, 5.72; N, 1.82. ^1H NMR (DMSO-d_6) in δ (ppm): 4.10 and 3.93 (4H, 2s), 1.60 (3H, s) along with the peaks from PPN^+ cation.

Identification of $(\eta^5\text{-MeCp})Mn(CO)_2(PR_3)$ (R=Me, Et, OEt, C_6H_5). To a N_2-filled 100 mL Schlenk flask was loaded $PPN^+(\eta^5\text{-MeCp})Mn(CO)_2Cl^-$ (1.0 mmol), followed by the addition of a 40 mL portion of degassed THF *via* syringe. PR_3 was added to the dark-red solution, and the reaction mixture was heated in a water bath at 60 ℃. The progress of the reaction was monitored by the ν(CO)IR bands of the product, $(\eta^5\text{-MeCp})Mn(CO)_2(PR_3)$ (R=OEt, C_6H_5) (10-12 hr). The other reaction products $(\eta^5\text{-MeCp})Mn(CO)_2(PR_3)$ (R=Me, Et) were quickly obtained on mixing the reactants, which confirmed by the IR spectroscopy. The vacuum-dried reaction mixtures were extracted into hexane and passed through a Celite-containing glass filter to isolate the PPN^+Cl^-. The hexane was removed under vacuum from the yellow filtrate at about 60 ℃ yielding a yellow oily mixture. Thin layer chromatography under nitrogen of a drop of this oil on a silica gel plate (Whatman #4420-222) in a 4 : 1 hexane-THF mixture shows the presence of $(\eta^5\text{-MeCp})Mn(CO)_3$ (Rf=0.88), $(\eta^5\text{-MeCp})Mn(CO)_2[P(C_6H_5)_3]$ (Rf=0.71), $[P(C_6H_5)_3]$ (Rf=0.03). The orange-colored product extracted from the yellow oil by the column chromatography under nitrogen turned out to be $(\eta^5\text{-MeCp})Mn(CO)_2[P(C_6H_5)_3]$. The eluent used was a 4 : 1 hexane-THF mixture. The other products $(\eta^5\text{-MeCp})Mn(CO)_2(PR_3)$ (R=Et, Me, OEt) were obtained as pure compounds under vacuum. The spectroscopic data are as follows: **$(\eta^5\text{-MeCp})Mn(CO)_2(PEt_3)$**: ν(CO)IR (THF) in cm^{-1}: 1918 (s), 1852 (s). ^1H NMR (CD_3OD) in δ (ppm): 4.35 (4H, d), 1.99 (3H, s), 1.71 (6H, m), 1.12 (9H, m). Mass, m/e [relative intensity, assignment]: 308 [14, $(\eta^5\text{-MeCp})Mn(CO)_2(PEt_3)$], 252 [100, $(\eta^5\text{-MeCp})Mn(PEt_3)$], 134 [32, $(\eta^5\text{-MeCp})Mn$]. **$(\eta^5\text{-MeCp})Mn(CO)_2(PMe_3)$**: ν (CO)IR (THF) in cm^{-1}: 1915 (s), 1849 (s). ^1H NMR (DMSO-d_6) in δ (ppm): 4.44 (4H, d), 1.88 (3H, s), 1.39 (9H, d). Mass, m/e [relative intensity, assignment]: 266 [10, $(\eta^5\text{-MeCp})Mn(CO)_2(PMe_3)$], 210 [85, $(\eta^5\text{-MeCp})Mn(PMe_3)$], 134 [100, $(\eta^5\text{-MeCp})Mn$]. **$(\eta^5\text{-MeCp})Mn(CO)_2[P(OEt)_3]$**: ν (CO)IR (THF) in cm^{-1}: 1935 (s), 1870 (s). ^1H NMR (DMSO-d_6) in δ (ppm): 4.47 (4H, s), 3.85 (6H, m), 1.87 (3H, s), 1.19 (9H, m). Mass, m/e [relative intensity, assignment]: 356[13, $(\eta^5\text{-MeCp})Mn(CO)_2[P(OEt)_3]$], 300 [100, $(\eta^5\text{-MeCp})Mn[P(OEt)_3]$], 134 [44, $(\eta^5\text{-MeCp})Mn$]. **$(\eta^5\text{-MeCp})Mn(CO)_2(PPh_3)$**: ν (CO)IR (THF) in cm^{-1}: 1927 (s), 1963 (s). ^1H NMR ($CDCl_3$) in δ (ppm): 7.56 (15H, m), 4.18 and 4.04 (4H, 2s), 1.93 (3H, s). Mass, m/e [relative intensity, assignment]: 452 [6.34, $(\eta^5\text{-MeCp})Mn(CO)_2(PPh_3)$], 396 [100, $(\eta^5\text{-MeCp})Mn(PPh_3)$], 134 [39, (η5-MeCp)Mn].

Kinetic Measurements. The kinetic experiments were carried out in a dried 10 mL volumetric flask securely fitted with a rubber septum. In a typical kinetic experiment, 0.05 mmol of an anionic transition metal carbonyl complex was loaded into a 10 mL volumetric flask in a drybox. The flask was removed from the drybox, and the respective THF solution of triethylphosphine, trimethylphosphine, triphenylphosphine, or triethylphosphite of known concentration was added by a syringe. This solution was stirred until it was homogeneous and placed in a Haake water bath equipped with a constant-temperature controller (± 0.1 ℃). Samples for IR spectral analysis were withdrawn periodically with a syringe and placed in a sealed 0.1 mm pathlength KBr or CaF_2 infra-

Table 1. Solution IR Spectral Data for $M^+(\eta^5\text{-MeCp})Mn(CO)_2Cl^-$ ($M^+ = K^+$, PPN^+, K^+(18-C-6)) and $(\eta^5\text{-MeCp})Mn(CO)_2PR_3$ (R= Me, Et, OEt, Ph) in THF

Complexes	ν(CO), cm^{-1}
$(\eta^5\text{-MeCp})Mn(CO)_3$	2010(s), 1924(s)
$(\eta^5\text{-MeCp})Mn(CO)_2(THF)$	1920(s), 1845(s)
$K^+(\eta^5\text{-MeCp})Mn(CO)_2Cl^-$	1891(s), 1814(s), 1802(s)
K^+(18-C-6)$(\eta^5\text{-MeCp})Mn(CO)_2Cl^-$	1895(s), 1816(s)
$PPN^+(\eta^5\text{-MeCp})Mn(CO)_2Cl^-$	1893(s), 1816(s)
$(\eta^5\text{-MeCp})Mn(CO)_2(PMe_3)$	1915(s), 1849(s)
$(\eta^5\text{-MeCp})Mn(CO)_2(PEt_3)$	1918(s), 1852(s)
$(\eta^5\text{-MeCp})Mn(CO)_2(P(OEt)_3)$	1935(s), 1870(s)
$(\eta^5\text{-MeCp})Mn(CO)_2(PPh_3)$	1927(s), 1863(s)

red solution cell. Rates of reaction were observed by following the disappearance in absorbance of the reactant's ν (CO) IR which did not overlap with the other carbonyl bands: $PPN^+(\eta^5\text{-MeCp})Mn(CO)_2Cl^-$ at 1816 cm^{-1}.

Under the pseudo-first-order reaction conditions, rate constants were calculated using a linear least-squares program for the first order rate plots of $[A_t\text{-}A_\infty]$ *vs* time, where A_t is the absorbance at time t and A_∞ is the absorbance at time infinity.

Results and Discussion

The synthesis of the anionic transition metal carbonyl complexes was achieved by the simple addition of labile ligand to the derivatives of group 7 metal carbonyls, $(\eta^5\text{-MeCp})Mn(CO)_2(THF)$ with PPN^+Cl^- or K^+(18-C-6)Cl^- as depicted in equation (4).

$$PPN^+Cl^-/CH_2Cl_2 + (\eta^5\text{-MeCp})Mn(CO)_2(THF) \rightarrow PPN^+(\eta^5\text{-MeCp})Mn(CO)_2Cl^- \quad (4)$$

The reactions were complete at time of mixing (ambient temperature), yielding products which were isolated by precipitation in 50 to 80% yield. The brown crystalline products were stable for a few days under nitrogen.

Comparison of the ν (CO)IR for $(\eta^5$-MeCp)Mn(CO)L (L=Cl^-, THF, CO, PMe_3, PEt_3, $P(OEt)_3$, PPh_3). For a series of analogous η^5-MeCp$Mn(CO)_2L$ (L=CO, Cl^-, PR_3; R=Me, Et, OEt, Ph) complexes, CO stretching frequencies are employed as a means to assess the relative electron density at the metal center. (See Table 1.) The assumption made here is that the increased electron density at Mn will be reflected by the increased back donation into the π^* orbital of the CO ligand resulting in lower ν (CO)IR (cm^{-1}). Based on this assumption, the relative electron donating ability of ligands is as follows:

$$Cl^- > PMe_3 \sim PEt_3 > THF > PPh_3 > P(OEt)_3 > CO$$

In the case of $M^+(\eta^5\text{-MeCp})Mn(CO)_2Cl^-$ ($M^+ = K^+$(18-C-6), PPN^+) in Table 1, two ν (CO)IR bands (1895, 1816 for $M^+ = K^+$(18-C-6) salt; 1893, 1816 for PPN^+ salt) were observed; however, the spectrum of $K^+(\eta^5\text{-MeCp})Mn(CO)_2Cl^-$ shows three bands (1891, 1814, 1802), among which one band (1802 cm^-) may be ascribed to the interaction between Mn-CO and K^+. (See Figure 1(a).) In this case, those contributions from the interactions depicted in Figure 1(b) and (c) may essentially be minimal because the stretching frequencies of the two peaks (1891, 1814 cm^{-1}) are not higher than those of K^+(18-C-6)$(\eta^5\text{-MeCp})Mn(CO)_2Cl^-$ (1895, 1816 cm^{-1}). Even the interaction shown in Figure 1(a) vanishes in the case of K^+(18-C-6) salt, where the crown ether (18-C-6) effectively interrupts the interaction by complexing K^+ cation.

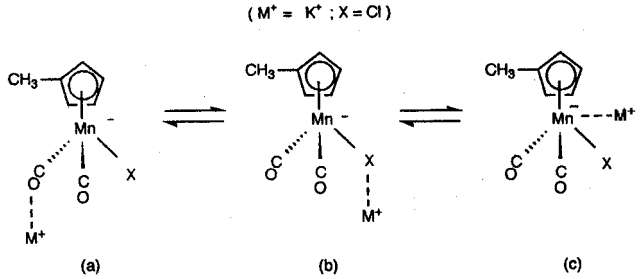

Figure 1. Interaction modes of cation with $(\eta^5\text{-MeCp})Mn(CO)_2Cl^-$ anion.

Table 2. The Relationship between $P(OEt)_3$ Concentrations and the Rates(k_{obs}) of the Reaction of $PPN^+(\eta^5\text{-MeCp})Mn(CO)_2Cl^-$ in THF at 50 ℃

$[PPN^+(\eta^5\text{-MeCp})Mn(CO)_2Cl^-]$ M(×10^3)	$[P(OEt)_3]$ M(×10^3)	$k_{obs}\times10^6$, s^{-1}
5.0	25	16.4± 0.7
5.0	50	18.7± 0.6
5.0	100	15.8± 0.4
5.0	200	16.4± 1.0

Table 3. The Relationship between PPh_3 Concentrations and the Rates(k_{obs}) of the Reaction of $PPN^+(\eta^5\text{-MeCp})Mn(CO)_2Cl^-$ in THF at 50 ℃

$[PPN^+(\eta^5\text{-MeCp})Mn(CO)_2Cl^-]$ M(×10^3)	$[PPh_3]$ M(×10^3)	$k_{obs}\times10^6$, s^{-1}
5.0	25	10.1± 0.4
5.0	50	10.1± 0.4
5.0	100	12.0± 0.4
5.0	200	13.0± 0.6

Reaction of $PPN^+(\eta^5$-MeCp)Mn(CO)$_2Cl^-$ with PR_3 (R=Et, Me, OEt, Ph). The reactions of $PPN^+(\eta^5\text{-MeCp})Mn(CO)_2Cl^-$ with an excess amount of PR_3 were carried out in THF solution at the various temperatures (r.t. to 60 ℃). The reaction products $(\eta^5\text{-MeCp})Mn(CO)_2(PR_3)$ were obtained as depicted in equation (5).

$$PPN^+(\eta^5\text{-MeCp})Mn(CO)_2Cl^- + PR_3 \rightarrow (\eta^5\text{-MeCp})Mn(CO)_2(PR_3) + PPN^+Cl^- \quad (5)$$

Reactions of $PPN^+(\eta^5\text{-MeCp})Mn(CO)_2Cl^-$ with an excess of PR_3 (5 up to 40-fold excess compared with the concentration of the complex) were performed in THF and monitored with time by ν (CO)IR (Table 2, 3). As is shown in Table

Table 4. Temperature Dependence on the Rate of the Reaction of $PPN^+(\eta^5\text{-MeCp})Mn(CO)_2Cl^-$ with $P(OEt)_3$ in THF[a]

Complex	Temp. (℃)	$k_{obs}\times10^6$, s^{-1}
$PPN^+(\eta^5\text{-MeCp})Mn(CO)_2Cl^-$	40	6.4± 0.2
	45	10.1± 0.6
	50	16.4± 1.0
	60	45.2± 1.5

[a] $[PPN^+(\eta^5\text{-MeCp})Mn(CO)_2Cl^-]=5.0$ mM; $[P(OEt)_3]=100$ mM.

Table 5. Temperature Dependence on the Rate of the Reaction of $PPN^+(\eta^5\text{-MeCp})Mn(CO)_2Cl^-$ with PPh_3 in THF[a]

Complex	Temp. (℃)	$k_{obs}\times10^6$, s^{-1}
$PPN^+(\eta^5\text{-MeCp})Mn(CO)_2Cl^-$	40	4.3± 0.2
	45	6.8± 0.3
	50	12.0± 0.4
	60	34.5± 0.9

[a] $[PPN^+(\eta^5\text{-MeCp})Mn(CO)_2Cl^-]=5.0$ mM; $[PPh_3]=100$ mM.

Table 6. Activation Parameters from the Reaction of $PPN^+(\eta^5\text{-MeCp})Mn(CO)_2Cl^-$ with PR_3 (R=OEt, Ph) in THF[a]

Ligand	Activation Parameters
$P(OEt)_3$	$\Delta H^{\ddagger}=19.8\pm0.6$ kcal/mol
	$\Delta S^{\ddagger}=-19.3\pm1.8$ e.u.
PPh_3	$\Delta H^{\ddagger}=21.0\pm1.5$ kcal/mol
	$\Delta S^{\ddagger}=-16.4\pm4.6$ e.u.

[a] $[PPN^+(\eta^5\text{-MeCp})Mn(CO)_2Cl^-]=5.0$ mM; $[PR_3]=100$ mM.

2 (for $P(OEt)_3$) and Table 3 (for PPh_3), each reaction follows a first order dependence on $[(\eta^5\text{-MeCp})Mn(CO)_2Cl^-PPN^+]$ and no dependence on $[PR_3]$, (R=OEt, Ph) within the experimental error range.

$$\text{rate}=k_1\ [PPN^+(\eta^5\text{-MeCp})Mn(CO)_2X^-] \qquad (6)$$

The reaction rate was also observed to be enhanced with temperature (Table 4, 5) under the pseudo-first-order conditions.

Determination of Activation Parameters. The first order rate constants, k_1, were measured for the reaction of $PPN^+(\eta^5\text{-MeCp})Mn(CO)_2Cl^-$ with PR_3 (R=OEt, Ph) in THF as a function of temperature and the activation parameters were calculated from the Eyring plot. The activation parameters ($\Delta H^{\ddagger}=19.8\pm0.6$ kcal/mol, $\Delta S^{\ddagger}=-19.3\pm1.8$ e.u. for $P(OEt)_3$; $\Delta H^{\ddagger}=21.0\pm1.5$ kcal/mol, $\Delta S^{\ddagger}=-16.4\pm4.6$ e.u. for PPh_3, see Table 6) both suggest that the associative ligand substitution may take place at the rate-determing step. However, the rate solely depends on the concentration of the metal complex. These two apparently opposite results may be compromised by the introduction of the coordinating solvent, THF. The $PPN^+(\eta^3\text{-MeCp})Mn(CO)_2Cl^-$ on heating may accomodate a THF molecule first, as is represented by the negative entropy change of activation and the overall first-order dependence on the concentration of the metal complex as well.

Table 7. Ligand Dependence on the Reaction of $PPN^+(\eta_5\text{-MeCp})Mn(CO)_2Cl^-$ with PR_3 (R=Me, Et, OEt, Ph) in THF[a]

Ligand	Temp. (℃)	Ligand Cone Angle (°)	$k_{obs}\times10^6$, s^{-1}
PMe_3	20	118	b
PEt_3	20	132	b
$P(OEt)_3$	40	106	6.4± 0.2
PPh_3	40	142	4.3± 0.2

[a] $[PPN^+(\eta^5\text{-MeCp})Mn(CO)_2Cl^-]=5.0$ mM; $[PR_3]=100$ mM. [b] These reactions are too fast to measure the rates by the method used here.

Mechanistic Considerations. It looks rather surprising to observe that the incoming ligand PR_3 (R=Me, Et, OEt, C_6H_5) does have the major effect on the reaction rate as shown in Table 7.

It is generally accepted that in the associative ligand substitution reactions, there is a pronounced steric retardation with the increasing cone angle of PR_3, regardless of phosphine basicity; however, in this reaction, the dominant factor contributing to the enhanced reaction rate appears to be the basicity (or nucleophilicity) of the ligand, PR_3, definitely not the steric factor of the ligand.[3c] The fact that electronic factor of the incoming ligand determines the rate may partly be related to the electronic environment of the site for attack, Mn, by the incoming ligand. The manganese metal center should be electron-deficient, to some degree, at the time of attack by the ligand; therefore the better σ-donating ligand could more effectively attack the metal center than the other ligands ($P(OEt)_3$, $P(C_6H_5)_3$) do.

The relatively low electron density buildup on the Mn center could be achieved through the structural reorganization, where an appropriate energy is applied; e.g., the shift from η^5-MeCp to η^3-MeCp creating an open coordination site[5] and also the electron density on Mn can be pulled over by the electron withdrawing ligand, Cl^-, simultaneously.

This $\eta^3\text{-MeCpMn(CO)}_2Cl^-PPN^+$, although it is a charged species, is assumed to be a 16 electron species; therefore, this complex may accomodate another two electron donor ligand, either the coordinating solvent, THF, or PR_3. However, the Mn-Cl bond should be cleaved with the formation of PPN^+Cl^- leading to the stable neutral intermediate, $\eta^5\text{-MeCpMn(CO)}_2$(THF) prior to the attack at the metal center by PR_3 ligand.

The intermediate $(\eta^5\text{-MeCp})Mn(CO)_2$(THF) can survive for hours at ambient temperature under N_2. At this stage, the electronic factor of the ligand, PR_3, may be little related to the reaction rate because the neutral intermediate, $\eta^5\text{-MeCpMn(CO)}_2$(THF), no longer demands either steric or electronic enhancements from the PR_3.

As no kinetic data could be obtained from the reactions with the PR_3 (R=Me, Et) due to the very fast reaction, (These reactions cannot be followed by the ν (CO) IR spectroscopic method employed here) it does not yet appear to be certain whether these reactions with PR_3 (R=Me, Et) are in the associative ligand substitution mode or not; however, the incredibly fast reaction ($k_{obs}\cong1.7\times10^{-2}$ s^{-1} for PMe_3 at 1 : 1 molar ratio with respect to $[(MeCp)Mn(CO)_2Cl^-]$ at ambient temperature; this reaction rate is almost 10^3 times

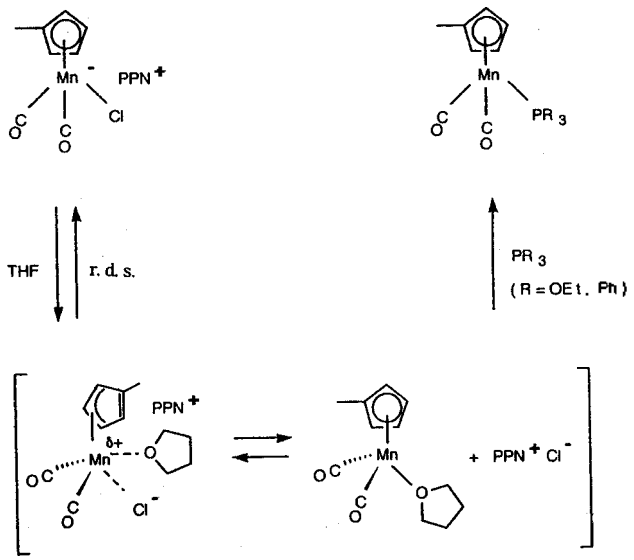

Figure 2. Proposed reaction sequencies for $PPN^+(\eta^5\text{-MeCp})Mn(CO)_2Cl^-$ with PR_3 (R=Me, Et, OEt, Ph).

faster than that for $P(OEt)_3$. See Table 3) may drive us to believe that the strong nucleophile, PR_3 (R=Me, Et) may directly attack at the Mn center of the $PPN^+(\eta^3\text{-MeCp})Mn(CO)_2Cl^-$ to yield the corresponding product, η^5-MeCpMn $(CO)_2(PR_3)$. Therefore, the reaction mechanism involving a dissociative ligand substitution seems to be related to the weak nucleophilicity of the incoming ligand, PR_3 (Figure 2). This situation may as well be compared with the nucleophilic substitution reactions (S_N1 *vs* S_N2) depending on the structure of the substrate and the nucleophilicity of the nucleophile involved. More in-depth fast kinetic study at low temperature on the same reaction with PR_3 (R=Me, Et, etc.) should be done later in the near future.

Acknowlegment. This research was supported by the Korea Science and Engineering Foundation (92-25-00-04). Authors greatly appreciate those (M. S. Kim and Y. K. Park) for their help in preparing this manuscript. Y. K. P thanks Professor S. H. Lee for the GC-MASS data collections. Authors thank one of the referees for the valuable advice regarding the mechanistic considerations.

References

1. (a) Dessy, R. E.; Pohl, R. L.; King, R. B. *J. Am. Chem. Soc.* **1966**, *88*, 5121. (b) Collman, J. P. *Acc. Chem. Res.* **1975**, *8*, 342. (c) Darensbourg, M. Y.; Darensbourg, D. J.; Drew, D. A.; Burus, D. *J. Am. Chem. Soc.* **1976**, *98*, 3127. (d) Moro, A.; Foa, M., Cassar, L. *J. Organomet. Chem.* **1980**, *212*, C 68. (e) Darensbourg, M. Y.; Jimmenez, P.; Sackett, J. R.; Hankel, J. M.; Kump, R. L. *J. Am. Chem. Soc.* **1982**, *104*, 1521. (f) Watson, P. L; Bergman, R. G. *J. Am. Chem. Soc.* **1979**, *101*, 2055.
2. (a) Park, Y. K.; Han, I. S.; Huh, T. S. *Bull. Korean Chem. Soc.* **1990**, *11*, 221. (b) Park, Y. K.; Kim, S. J.; Kim, J. H.; Han, I. S.; Lee, C. H.; Choi, H. S. *J. Organomet. Chem.* **1991**, *408*, 193.
3. (a) Ji, L. N.; Rerek, M. E.; Basolo, F. *Organometallics* **1984**, *3*, 740. (b) Rerek, M. E.; Basolo, F. *Organometallics* **1983**, *2*, 372. (c) Kakkar, A. K.; Taylor, N. J.; Marder, T. B. *Inorg Chim Acta*, **1992**, *198*, 219. (d) Glueck, D. S.; Bergman, R. G. *Organometallics* **1991**, *10*, 1479. (e) Halabi, M. A.; Atwood, J. D.; Forbus, N. P.; Brown, T. L. *J. Am. Chem. Soc.* **1980**, *102*, 6248.
4. (a) Butler, I. S.; Coville, N. J.; Cozak, D. *Inorg. Synth.* **1978**, *19*, 188. (b) Nyholm, R. S.; Sabdhu, S. S.; Stiddard, M. H. B. *J. Chem. Soc.* **1963**, *92*, 5916.
5. (a) Rerek, M. E.; Ji, L. N.; Basolo, F. *J. Chem. Soc., Chem. Commun.* **1983**, 1208. (b) Hart-Davis, A. J.; Mawby, R. J. *J. Chem. Soc. A* **1969**, 2403.
6. (a) Tolman, C. A. *J. Am. Chem. Soc.* **1970**, *92*, 2956. (b) Tolman, C. A. *Chem. Soc. Rev.* **1972**, *1*, 337.